Vortex nucleation induced phonon radiation from a moving electron bubble in superfluid ^{4}He

Dafei Jin[1] and Wei Guo[2]
[1]*Department of Physics, Brown University, Providence, Rhode Island 02912, USA*
[2]*Department of Physics, Yale University, New Haven, Connecticut 06520, USA*
(Received 9 July 2010; published 30 September 2010)

We construct an efficient zero-temperature semilocal density functional to dynamically simulate an electron bubble passing through superfluid ^{4}He under various pressures and electric fields up to nanosecond time scale. Our simulated drift velocity can be quantitatively compared to experiments particularly when pressure approaches zero. We find that the high-speed bubble experiences remarkable expansion and deformation before vortex nucleation occurs. Accompanied by vortex-ring shedding, drastic surface vibration is generated leading to intense phonon radiation into the liquid. The amount of energy dissipated by these phonons is found to be greater than the amount carried away solely by the vortex rings. These results may enrich our understanding about the vortex nucleation induced energy dissipation in this fascinating system.

DOI: 10.1103/PhysRevB.82.094524 PACS number(s): 67.25.dg, 67.25.dk

I. INTRODUCTION

An electron injected into liquid helium forms a bubble due to the Pauli exclusion between an excess electron and helium atoms.[1,2] The dissipation mechanisms of a moving electron bubble in superfluid ^{4}He has attracted considerable research interests for many years.[3–11] Above 1 K, the moving bubble experiences a drag force from collisions with thermally excited phonons and rotons.[3] Below 1 K, this drag force becomes very small, and even a weak electric field can accelerate the bubble to a high speed until some new dissipation mechanisms set in. In the high-pressure regime, roton emission dominates the dissipation owing to the relatively low Landau velocity v_L and the high vortex-ring nucleation critical velocity v_c.[4,5] In the low-pressure regime, vortex-ring nucleation plays the key role. A vortex ring can attach to the bubble to form a bubble-ring complex if the electric field is not overly strong; otherwise, successive vortex rings can be shed away from the bubble surface.[6–8]

Pioneering simulations using the Gross-Pitaevskii equation (GPE) have demonstrated the above vortex-ring nucleation, trapping, and shedding scenario.[12,13] But it is known to be difficult for the efficient local GPE to reproduce helium properties.[14] In contrast, accurate nonlocal density functional theories have been extensively applied to quasiparticles, vortices, and ions-related problems in liquid helium.[15,16] But they usually require prohibitively high computational cost for dynamic simulations. In this paper, we introduce our well-constructed semilocal density functional (SLDF), associated with an optimized numerical scheme, that can reconcile both the physical accuracy and the computational efficiency in its applicable regime.[17,18] We then present our dynamic simulation for a moving electron bubble in pure superfluid ^{4}He under low pressures and strong electric fields, where successive vortex-ring shedding is indeed observed. However, we shall point out that although vortex nucleation does trigger the dissipation, the major part of energy loss may come from its induced phonon radiation via surface vibration, rather than purely the shed-away vortex rings.

II. THEORETICAL FORMULATION

We formulate our problem in the framework of a zero-temperature SLDF theory. The system free-energy density $\mathcal{G}$ consists of the helium part, the electron part, and the helium-electron interaction part,

$$\mathcal{G} = \mathcal{G}_{\mathrm{He}} + \mathcal{G}_{\mathrm{e}} + \mathcal{G}_{\mathrm{He\text{-}e}}. \tag{1}$$

The helium part $\mathcal{G}_{\mathrm{He}}$ takes the form of

$$\begin{aligned}\mathcal{G}_{\mathrm{He}} = {} & \frac{\hbar^2}{2m_{\mathrm{He}}}|\nabla\psi|^2 - \mu\varrho \\ & + \frac{1}{2}g_2\varrho^2 + \frac{1}{3}g_3\varrho^3 + \frac{1}{4}g_4\varrho^4 \\ & + \frac{1}{2}h_2|\nabla\varrho|^2 + \frac{1}{3}h_3\varrho|\nabla\varrho|^2 + \frac{1}{4}h_4\varrho^2|\nabla\varrho|^2,\end{aligned} \tag{2}$$

where ψ is the macroscopic helium wave function and $\varrho \equiv |\psi|^2$ is the local helium number density. The electron part $\mathcal{G}_{\mathrm{e}}$ takes the form of

$$\mathcal{G}_{\mathrm{e}} = \frac{\hbar^2}{2m_{\mathrm{e}}}|\nabla\phi|^2 - e\mathcal{E}z\eta, \tag{3}$$

where ϕ is the single-electron wave function and $\eta \equiv |\phi|^2$ is the local electron number density. The $|\nabla\psi|^2$ and $|\nabla\phi|^2$ terms above are the helium and electron kinetic energy densities, with m_{He} and m_{e} being the helium and electron masses, respectively. μ is the helium chemical potential controlled by a given pressure p, which fixes the helium number density ρ in bulk. $\mathcal{E}$ is the applied electric field, which drives the electron to move along z direction. g_2, g_3, g_4 and h_2, h_3, h_4 are all fitting parameters to be explained below. The helium-electron interaction part $\mathcal{G}_{\mathrm{He\text{-}e}}$ takes the form of a contact collision,

$$\mathcal{G}_{\mathrm{He\text{-}e}} = f_1\varrho\eta, \tag{4}$$

in which f_1 is a fitting parameter chosen so as to produce a 1 Å scattering length and hence a 1.0456 eV potential barrier for an electron to tunnel into homogeneous helium at zero temperature and zero pressure.[1,2]

The polynomial function of ϱ in the second line of Eq. (2) is the helium-helium interaction energy density in the form of two-particle, three-particle, and four-particle contact col-

lisions. In the homogeneous case, it gives the helium internal energy density,

$$\varepsilon[\rho] = \frac{1}{2}g_2\rho^2 + \frac{1}{3}g_3\rho^3 + \frac{1}{4}g_4\rho^4, \tag{5}$$

from which one can derive the equation of state,

$$p[\rho] = \frac{1}{2}g_2\rho^2 + \frac{2}{3}g_3\rho^3 + \frac{3}{4}g_4\rho^4, \tag{6}$$

the chemical potential

$$\mu[\rho] = g_2\rho + g_3\rho^2 + g_4\rho^3, \tag{7}$$

and the sound velocity

$$c[\rho] = \sqrt{(g_2\rho + 2g_3\rho^2 + 3g_4\rho^3)/m_{\mathrm{He}}}. \tag{8}$$

By choosing g_2, g_3, and g_4 according to the well-known Orsay-Trento density functional,[15] the experimentally measured above quantities at zero temperature can be very well produced.

The mixture polynomial function of ϱ and $|\nabla\varrho|^2$ in the third line of Eq. (2) contains our introduced semilocal interactions also up to four-particle collisions. They are the lowest-order gradient-expansion corrections to the local interactions and are essential for incorporating the helium surface tension into our theory,

$$\sigma[\rho] = \int_0^\rho d\varrho b[\varrho]\sqrt{\frac{\hbar^2}{8m_{\mathrm{He}}\varrho}} \times \frac{2(\varepsilon[\varrho] - \varepsilon[\rho]) - (\mu[\rho] + \varepsilon[\rho]/\rho)(\varrho - \rho)}{\sqrt{(\varepsilon[\varrho] - \varepsilon[\rho]) - \mu[\rho](\varrho - \rho)}}, \tag{9}$$

where the dimensionless function

$$b[\rho] = \sqrt{1 + \frac{8m_{\mathrm{He}}\rho}{\hbar^2}\left(\frac{1}{2}h_2 + \frac{1}{3}h_3\rho + \frac{1}{4}h_4\rho^2\right)}. \tag{10}$$

By choosing h_2, h_3, and h_4 appropriately, the experimentally measured surface tension at zero temperature and zero pressure can be produced. In addition, Eq. (9) is a generalized formula to allow not only zero pressure, when the liquid is in equilibrium with vacuum, but also a positive pressure, when the liquid is in contact with an impenetrable wall. In both situations, the liquid density drops from its bulk value ρ to 0 within a thin interfacial layer. $\sigma[\rho]$ measures the energy change per unit surface area due to this density bending, in comparison with the internal energy per unit area held by the same number of particles in bulk.[17] Such a generalized definition on the surface tension turns out to be useful for the electron bubble problem, where the bubble boundary pushes away the liquid basically like an impenetrable wall, and so gives rise to a nontrivial surface energy under any finite pressures.[2]

Table I lists all the chosen fitting parameters of our SLDF. Figure 1(a) shows the equation of state. At $p=0$ bar, $\rho_0 = 0.021836$ Å^{-3}, $\mu_0 = -7.1500$ K, and $c_0 = 237.70$ m s^{-1}. Figure 1(b) shows the surface tension versus pressure. At $p=0$ bar, $\sigma_0 = 0.37554$ erg cm^{-2} with a calculated 5.8 Å surface thickness (defined by 10–90 % helium density) consistent with experiments and other theories.[15,17,19]

TABLE I. The chosen fitting parameters of our SLDF.

Parameter	Value	Unit
f_1	5.55671×10^5	K Å^3
g_2	-7.18990×10^2	K Å^3
g_3	-3.61779×10^4	K Å^6
g_4	2.47799×10^6	K Å^9
h_2	1.16950×10^4	K Å^5
h_3	-1.35048×10^6	K Å^8
h_4	3.46549×10^7	K Å^{11}

The excitation spectrum in our theory can be found to be of the Bogoliubov type,

$$\hbar^2\omega^2 = c^2[\rho]\hbar^2k^2 + b^2[\rho]\left(\frac{\hbar^2k^2}{2m_{\mathrm{He}}}\right)^2, \tag{11}$$

whose pressure dependence is enclosed in the sound velocity $c[\rho]$ from the local interactions, and the dimensionless function $b[\rho]$ from the semilocal interactions. Compared with the efficient local GPE, although our SLDF can indeed produce more realistic helium bulk and surface properties, and meanwhile maintain the same computational efficiency, it still cannot incorporate the backflow effect and the roton excitation unless some nonlocal interactions are introduced.[14,15] Figure 1(c) shows the excitation spectrum under three typical pressures: the spinodal pressure −9.5 bar, the saturation pressure 0 bar, and the melting pressure 25 bar. The primary reason for employing three semilocal parameters, h_2, h_3, and h_4, in our SLDF instead of a single one, as that done in the well-known Stringari-Treiner density functional,[17] is to remove some pathological behavior of the excitation spectrum. A single semilocal parameter being used to fit the surface tension at zero pressure will result in too large of a $b[\rho]$ and hence unrealistically high excitation energies even at just moderate momentums.[18] This will make the liquid overrigid against density fluctuation and may bring on artifacts in dynamic simulations. With the three semilocal parameters, we can keep $b[\rho]$ sufficiently small, and also let it slowly decrease with pressure to imitate the tendency of roton gap with pressure in real helium.

We can also find in our theory the rectilinear vortex-line energy per unit length, by calculating the radial number density distribution $\varrho(r)$ under a given pressure,

$$\frac{E_{\mathrm{line}}}{L} = \int 2\pi r dr\left(\frac{\hbar^2}{2m_{\mathrm{He}}r^2}\varrho + p - \mu\varrho + \frac{1}{2}g_2\varrho^2 + \frac{1}{3}g_3\varrho^3 + \frac{1}{4}g_4\varrho^4 + \frac{\hbar^2}{8m_{\mathrm{He}}\varrho}\varrho'^2 + \frac{1}{2}h_2\varrho'^2 + \frac{1}{3}h_3\varrho\varrho'^2 + \frac{1}{4}h_4\varrho^2\varrho'^2\right), \tag{12}$$

where ϱ drops from its bulk value ρ to 0 as $r\to0$, and $\varrho' \equiv d\varrho/dr$. The first term in the first line contributes to the kinetic energy K_{line}/L due to one unit of quantum circulation.

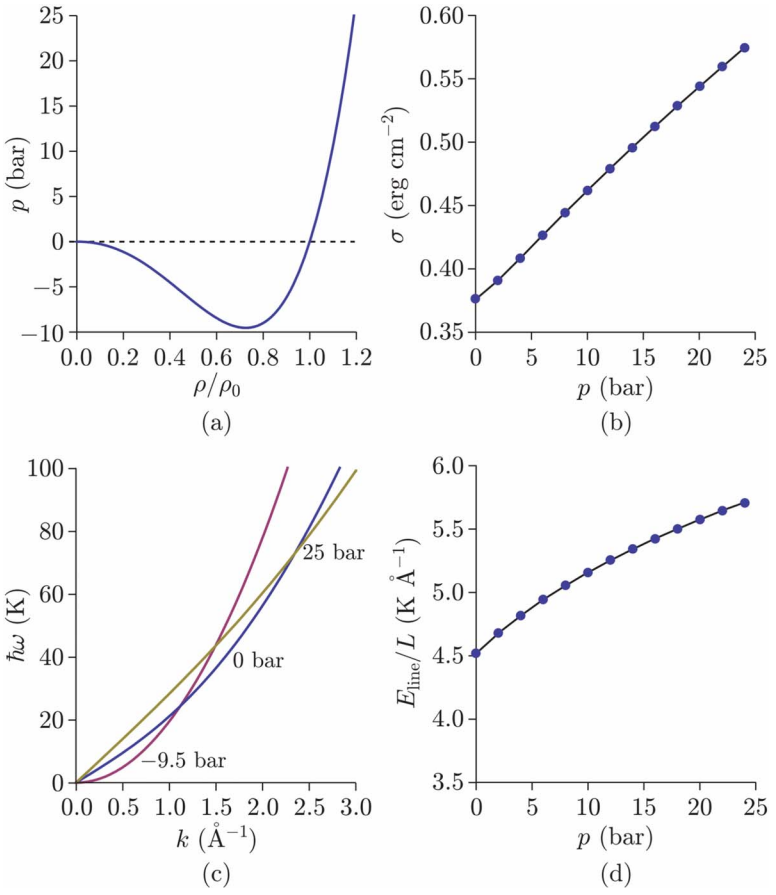

FIG. 1. (Color online) The helium properties in our SLDF. (a) The equation of state. (b) The surface tension versus pressure. (c) The excitation spectrum under the spinodal pressure −9.5 bar, the saturation pressure 0 bar, and the melting pressure 25 bar. (d) The vortex-line energy per unit length versus pressure with a 20 Å cutoff radial distance.

All the other terms contribute to the potential energy U_{line}/L due to the density bending.[20] The critical negative pressure for the free expansion of a vortex core is found to be close to −7 bar. Figure 1(d) shows the vortex-line energy per unit length versus pressure with a $d=20$ Å cutoff radial distance. At $p=0$ bar, we find $K_{\text{line}}/L=2.94$ K Å^{-1} and $U_{\text{line}}/L=1.57$ K Å^{-1}. Putting them into the hollow-core model,[10]

$$\frac{K_{\text{line}}}{L}=\frac{\pi\hbar^2}{m_{\text{He}}}\rho_0 \ln\frac{d}{a},$$

$$\frac{U_{\text{line}}}{L}=\frac{\pi\hbar^2}{m_{\text{He}}}\rho_0\delta, \tag{13}$$

we can get the core size $a=0.581$ Å and the core parameter $\delta=1.893$, which imply a rather rigid core.

III. DYNAMIC SIMULATION

We perform the dynamic simulation in the experimental low-pressure regime $p=0-10$ bar and strong electric field regime $\mathcal{E}=1-30$ MV m^{-1}. Under these conditions, a high-speed electron bubble can nucleate vortex rings. As is well known, there are two classic models on the formation of a vortex ring and a bubble-ring complex.[9–11] One is the encircling-ring (quantum transition) model, in which a full ring axisymmetrically appears on the bubble equator first, then moves sideways and captures the bubble on its core. The other one is the pinned-ring (peeling) model, in which a small proto-ring nonaxisymmetrically appears on the bubble equator first, then grows up and retains the bubble on its core. Experimental evidence suggests that the encircling-ring model gives a better description at lower temperatures in isotopically purified ^{4}He, whereas the pinned-ring model gives a better description at higher temperatures in natural ^{4}He, with the existence of thermal rotons or ^{3}He impurities.[5–7] For an already formed bubble-ring complex, the strength of the electric field determines its subsequent behavior. In a field on the order of 10^3-10^4 V m^{-1}, the ring can keep trapping the bubble and may grow to micron size, which significantly hinders the bubble motion.[6] But in a field on the order of 10^6-10^7 V m^{-1}, owing to the vanishing escape barrier, the ring should separate from the bubble during several picoseconds with its size almost unchanged. The bubble can then move more freely, as well as successively shed away vortex rings.[8] Since our simulation is for pure ^{4}He at zero temperature, the axisymmetric vortex-ring nucleation in the encircling-ring model is more suitable. Furthermore, since our electric fields lie in the strong regime, the transient nonaxisymmetric capture-and-escape processes should have little influence on the long-time physics. Thus we reduce the original three-dimensional problem into two-dimensional by taking cylindrical symmetry with transverse coordinate r and longitudinal coordinate z. This simplification makes the numerical integration up to nanosecond time scale computationally practical.

The coupled equations of motion for the macroscopic helium wave function ψ and the single-electron wave function ϕ can be derived from our SLDF as

$$\dot{\psi} = -\frac{i}{\hbar}\left[-\frac{\hbar^2}{2m_{\mathrm{He}}}\nabla^2 - \mu + f_1|\phi|^2 + g_2|\psi|^2 + g_3|\psi|^4 + g_4|\psi|^6 - \left(\frac{1}{3}h_3 + \frac{1}{2}h_4|\psi|^2\right)(\nabla|\psi|^2 \cdot \nabla|\psi|^2) - \left(h_2 + \frac{2}{3}h_3|\psi|^2 + \frac{1}{2}h_4|\psi|^4\right)\nabla^2|\psi|^2\right]\psi,$$

$$\dot{\phi} = -\frac{i}{\hbar}\left[-\frac{\hbar^2}{2m_{\mathrm{e}}}\nabla^2 - e\mathcal{E}z + f_1|\psi|^2\right]\phi. \quad (14)$$

The fourth-order finite-difference method in space and the fourth-order Runge-Kutta method in time are used to do the numerical integration. The computation grid on the r-z plane is 500×1000 with the space step of 0.2 Å. So the physical space is a pipe of 200 Å in diameter and 200 Å in length. We let it move along to keep the electron in the center. Systematic numerical tests have been done to ensure that 0.2 Å spatial resolution provides enough precision for our problem, even when the vortex core structure is involved.

Due to the big difference between the helium and electron intrinsic time scales on the order of $m_{\mathrm{He}}/m_{\mathrm{e}}\sim7300$, we adopt the adiabatic approximation. For every instantaneous helium configuration, we first find the electron ground state by evolving the electron with 50 imaginary time steps of 0.001 fs, then develop helium with one real time step of 0.001 ps. To avoid the outgoing sound waves from the central region being reflected on the grid boundary, we set a space-dependent damping coefficient by replacing i with $\eta(s)+i$ in the helium equation of motion, where

$$\eta(s) = \frac{\bar{\eta}}{2}\left[1 + \tanh\left(\frac{s-\bar{s}}{\bar{w}}\right)\right], \quad (s \equiv \sqrt{r^2+z^2}). \quad (15)$$

We simply choose $\bar{s}=80$ Å, $\bar{w}=1.0$ Å, and $\bar{\eta}=0.5$. The sound waves can travel freely through the undamped region ($s<\bar{s}$) but are quickly attenuated in the damped region ($s>\bar{s}$). Physically, this looks as if there is a strong zero-temperature heat sink surrounding the system.

Figure 2 shows the calculated radial number density profiles of helium $\varrho(r)/\rho_0$ and electron $\eta(r)/\eta_\circ$ for a spherical static electron bubble under various pressures. Here $\eta_\circ \equiv \pi/2R_\circ^3$ with $R_\circ \equiv 20$ Å being merely a reference radius. The static bubble radius R_{b} (defined at 50% helium density) can be found to be 18.52 Å at $p=0$ bar and squeezed down to 13.50 Å at $p=10$ bar, consistent with experiments and other theories.[1,2] We set these ground states as the initial states to start the time evolution. For every single run with a specified pressure and electric field, eight-core parallel computation at 2.83 GHz was performed. Multiple runs with different pressures and electric fields were conducted simultaneously on our computing cluster which possesses hundreds of cores. Typically, it took about one month to reach 10 ns physical time.

Figure 3 shows the snapshots of the helium number density profile $\varrho(r,z;t)/\rho_0$ around the moving electron bubble at a sequence of times under $p=0$ bar and $\mathcal{E}=10$ MV m^{-1}. The instantaneous velocity v at each time is approximated by linearly fitting the displacement of the electron wave function maximum over a 20 ps time interval. At $t=0$ ps, the bubble is on its spherical ground state of radius $R_{\mathrm{b}}=18.52$ Å, when the driving field is just switched on. The initial acceleration of the bubble has the value that is expected based on the applied force $e\mathcal{E}$ and the hydrodynamic mass $2\pi R_{\mathrm{b}}^3 m_{\mathrm{He}}\rho_0/3$. Up until $t=40$ ps, v is already as high as 30.6 m s^{-1} whereas the bubble shape is only slightly squeezed and the liquid in front is slightly compressed. As the bubble velocity increases further, its volume keeps expanding and its shape keeps deforming into an oblate spheroid due to the negative pressure on the bubble waist caused by the Bernoulli effect.[21] The acceleration decreases remarkably because of the increase in the effective mass so that v approaches a constant value about 50.6 m s^{-1} and the flow pattern exhibits quite well fore-and-aft symmetry as shown at $t=450$ ps. After this stage, a narrow edge girdling the bubble waist gradually sticks out signifying the onset of vortex-ring nucleation. This adds a considerable inertia to the bubble motion, making v decrease to 44.9 m s^{-1} at $t=850$ ps, when the bubble attains its largest equatorial radius about 44 Å and its sharpest edge radius of curvature about 4 Å. We may call the bubble velocity for the first appearance of this characteristic behavior as the vortex-ring nucleation critical velocity $v_{\mathrm{c}}=44.9$ m s^{-1} under the prescribed conditions. There is no dissipation before since the electric work mainly transforms to the fluid kinetic energy. But around this time the liquid density starts to fluctuate accompanied by some phonon generation, presumably because the local flow near the bubble waist becomes supersonic and keeps hitting the nucleated vortex core.[12,13] At $t=950$ ps, a vortex ring of radius $R_{\mathrm{ring}}\approx36$ Å is detaching from the bubble surface while v is 43.8 m s^{-1} and continues to slow down due to the attraction from the vortex ring. The phonon generation appears more intense, particularly peaked at a wavelength of the order of 10 Å. The unexpected large ring radius, almost twice as big as the static bubble radius, is a unique observation of our dynamic SLDF simulation.

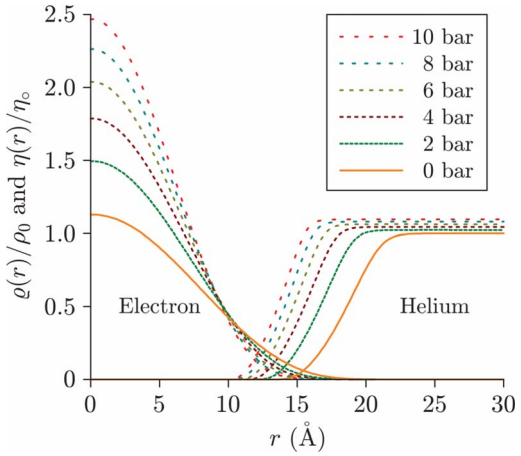

FIG. 2. (Color online) The radial number density profiles of helium and electron for a spherical static electron bubble under various pressures.

In the later stage, the vortex ring falls behind, leaving a drastic surface vibration and velocity oscillation to the bubble in the next hundreds of picoseconds. At $t=970$ ps, an

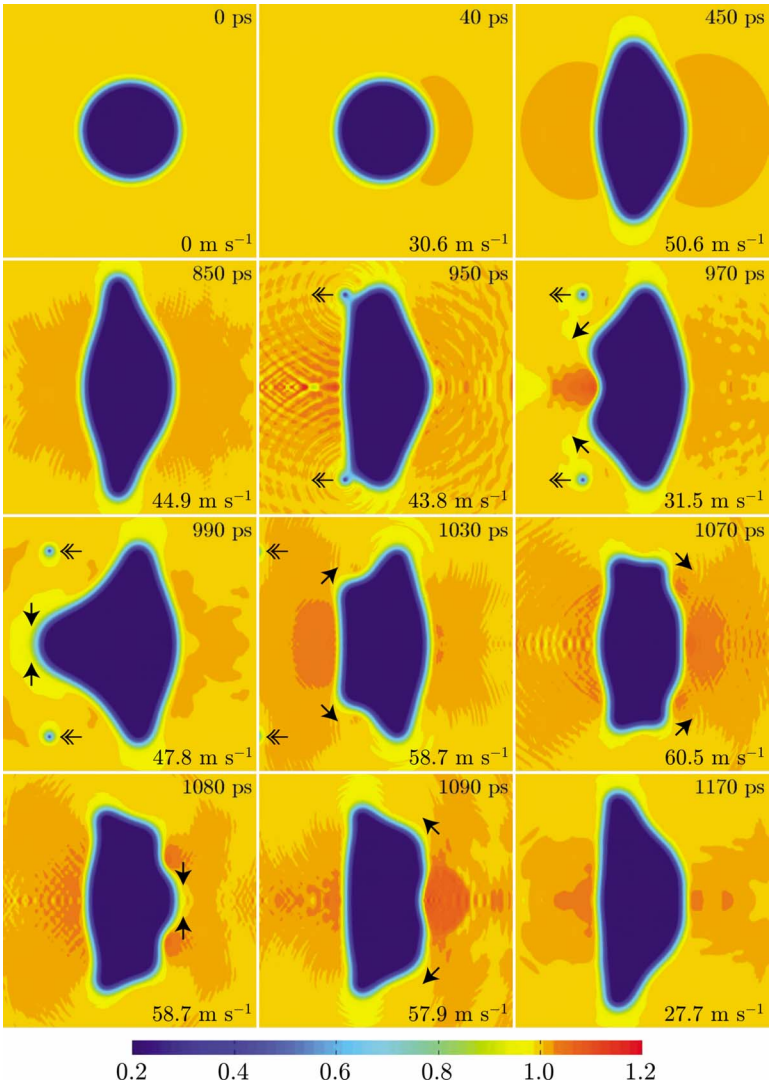

FIG. 3. (Color online) The snapshots of the helium number density profile around the moving electron bubble at a sequence of times under zero pressure and 10 MV m^{-1} electric field (Ref. 22). The bubble travels from left to right along z direction (the longitudinal direction). Each image corresponds to a physical size of 100 Å $\times$ 100 Å and is reflected up and down in r direction (the transverse direction) justified by the imposed cylindrical symmetry. The instantaneous velocity is given for each time. The open and solid arrows indicate the movements of vortex ring and solitary ripplon relative to the bubble as mentioned in the text.

annular surface protrusion like a solitary ripplon is formed and sliding backwards while v is dragged down to 31.5 m s^{-1}. This solitary ripplon then shrinks on the bubble tail at $t=990$ ps, and radiates a large number of phonons backwards into the liquid as shown at $t=1030$ ps. This provides a strong forward impulse to speed up the bubble so that v can even overshoot to 60.5 m s^{-1} at $t=1070$ ps. During this time, the solitary ripplon surviving from the last collision bounces back and propagates forward. Around $t=1080-1090$ ps, it shrinks on the bubble head and deposits a large number of phonons forward into the liquid. This provides a strong backward impulse decelerating the bubble velocity to as low as 27.7 m s^{-1} at $t=1170$ ps. Afterward, some remnant surface vibration and phonon radiation keep happening back and forth while the bubble velocity oscillatorily increases until a second vortex ring completes its nucleation. Then all the processes repeat.

IV. DISCUSSION

Figure 4 shows the time evolution of the moving electron bubble volume $V_b(t)/(4\pi R_b^3/3)$ under $p=0$ bar and $\mathcal{E}=10$ MV m^{-1}, obtained from the same evolution shown in Fig. 3 but extended to about 5 ns physical time. Here $4\pi R_b^3/3$ with $R_b=18.52$ Å is the spherical static bubble volume at $t=0$ ps. As can be seen, before the dissipation processes arise at $t\approx 850$ ps, $V_b(t)$ keeps growing to about 3.6 times the static volume. After that, $V_b(t)$ oscillates violently between 2.0 and 4.0 (average about 3.0) times the static volume. It approximately implicates the hydrodynamic mass variation, and coincides with the bubble velocity variation described above. The dotted lines mark the moments of the vortex-ring shedding events. During $t=800-5000$ ps, there are six such events in total. Although they do not exhibit a regular periodicity, we may still roughly estimate the average time interval between two successive events $\tau\approx 700$ ps. Each time when a ring leaves the bubble, there follows a huge volume change immediately and perhaps a series of small volume changes later on. This can be related to the complex surface motion displayed in Fig. 3.

Figure 5 shows the drift velocity $\bar{v}$ versus pressure under $\mathcal{E}=2.6$, 10, 20, and 30 MV m^{-1} from our simulation in comparison with the low-pressure part of experiment by Nancolas *et al.* at 0.3 K under 2.6 MV m^{-1}.[8] Our $\bar{v}$ is calculated by linearly fitting the displacement of the electron wave func-

tion maximum over 2 ns after the bubble motion has become strongly dissipative. Although the instantaneous velocity v mentioned above undergoes large oscillation, $\bar{v}$ is nearly constant depending only on the pressure and electric field for a long time. According to Nancolas *et al.*, if roton emission was the only dissipation mechanism, then in the limit $\mathcal{E} \rightarrow 0$ V m^{-1}, $\bar{v}$ should follow the dashed curve of Landau velocity v_L whereas for $\mathcal{E}=2.6$ MV m^{-1}, $\bar{v}$ should follow the dashed-dotted curve based on the well-known relation $\bar{v}=v_L+\mathcal{A}\mathcal{E}^{1/3}$, in which $\mathcal{A}$ takes its value at 25 bar with the pressure dependence ignored. However, the experimentally measured $\bar{v}$ shows a significant drop from this curve, indicating an additional dissipation mechanism in this low-pressure regime believed to be vortex-ring nucleation. Our work supports this general scenario especially for $p<3$ bar where the simulation and experimental results quantitatively agree with each other. This suggests that our SLDF can be an efficient and reliable tool to study interesting dynamic problems, particularly under the natural experimental condition $p \rightarrow 0$ bar close to zero temperature. The lack of roton excitation in our SLDF may not be problematic for two reasons that essentially prohibit roton emission in this range. First, the Landau velocity $v_L \approx 58$ m s^{-1} is substantially higher than the vortex-ring nucleation critical velocity $v_c \approx 45$ m s^{-1}. Second, there is experimental evidence that $\mathcal{A}$ is divergent as $p \rightarrow 3$ bar from above.[8] For $p>3$ bar, our simulation still exhibits a qualitatively correct behavior in terms of the increasing $\bar{v}$ with increasing p commonly understood as the inverse proportionality of v_c with respect to the bubble size.[9–12] The relatively large deviation between simulation and experiment is presumably caused by the lack of roton excitation in our SLDF whereas in reality, vortex-ring nucleation and roton emission coexist in this pressure range.

Although in Fig. 3 we have presented that vortex nucleation is indeed the origin of dissipation, it is nontrivial to investigate how the energy is actually taken away from the system. While this is normally attributed to purely the frequent vortex-ring shedding, our analysis suggests otherwise. The energy associated with a large single vortex ring at zero pressure can be estimated by[10]

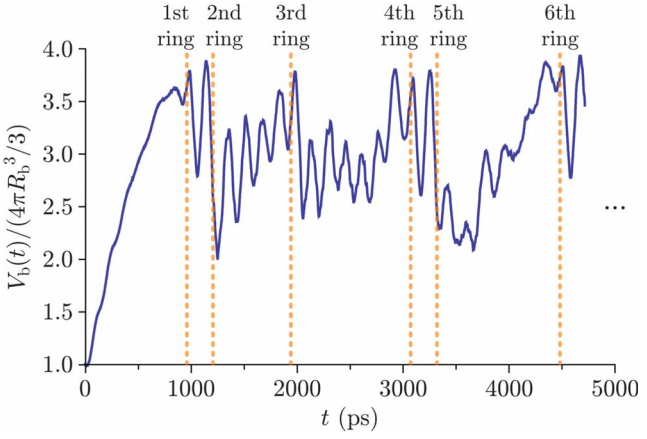

FIG. 4. (Color online) The time evolution of the moving electron bubble volume under zero pressure and 10 MV m^{-1} electric field. The dotted lines mark the moments of the vortex-ring shedding events.

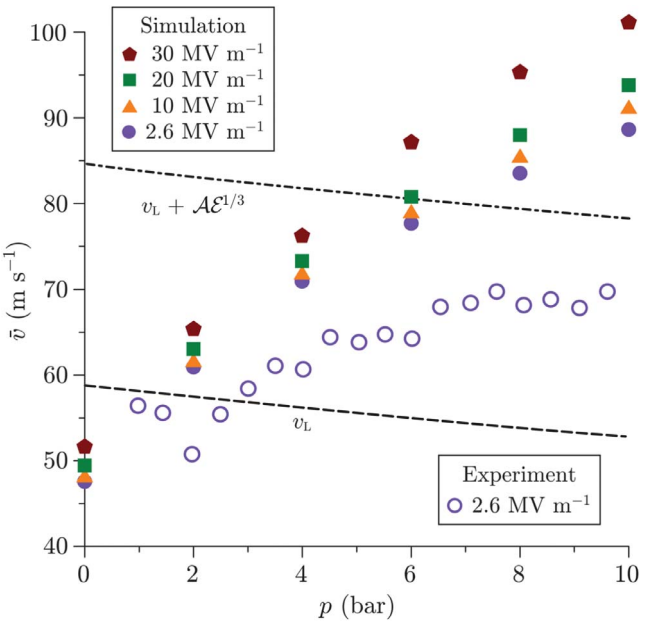

FIG. 5. (Color online) The drift velocity versus pressure under 2.6, 10, 20, and 30 MV m^{-1} electric fields from our simulation in comparison with the low-pressure part of experiment by Nancolas *et al.* at 0.3 K under 2.6 MV m^{-1}. The dashed curve gives the Landau velocity for roton emission. The dashed-dotted curve gives the theoretically extrapolated drift velocity from 25 bar under 2.6 MV m^{-1} if roton emission was the only dissipation mechanism (Ref. 8).

$$E_{\text{ring}} = \frac{\pi\hbar^2}{m_{\text{He}}}\rho_0 2\pi R_{\text{ring}}\left(\ln\frac{8R_{\text{ring}}}{a} - 2 + \delta\right). \tag{16}$$

Based on our preceding calculation about the vortex properties in our density functional, when $R_{\text{ring}} \approx 36$ Å as shown in Fig. 3, we have $E_{\text{ring}} \approx 1147$ K. As a result, the average rate of energy loss to the vortex rings is $E_{\text{ring}}/\tau \approx 1147$ K/700 ps$=2.3\times10^{-11}$ W. On the other hand, the average rate of energy input to the system from the electric work is $e\mathcal{E}\bar{v} \approx 10$ MeV m$^{-1}\times 48$ m s$^{-1}=7.7\times10^{-11}$ W. Strikingly, the released vortex rings only take away about 30% of the total input energy. According to the processes illustrated in Fig. 3 and discussed above, the remaining energy loss can be primarily attributed to the phonon radiation through surface vibration persistently occurring in the time interval between successive vortex-ring shedding events. Under a fixed electric field with an increasing pressure, we even notice a tendency for such a dissipation channel to become increasingly dominant.

V. CONCLUSION

We have carried out dynamic simulation for a moving electron bubble in pure superfluid ^{4}He under low pressures and strong electric fields, using a zero-temperature semilocal density functional theory that embodies realistic ^{4}He bulk and surface properties. It visualizes the underlying microscopic processes from picosecond to nanosecond time scale, which cannot yet be directly observed through any experi-

mental apparatus today. Not only have we confirmed that theory and experiment show good agreement on the bubble mobility approaching zero pressure, we have also discovered that the pronounced surface vibration and phonon radiation as a result of vortex nucleation dissipate more energy than the shed-away vortex rings alone. These results may enrich our understanding about the vortex nucleation induced energy dissipation in this fascinating system and so warrant further experimental and theoretical studies.

ACKNOWLEDGMENTS

The authors are very grateful to H. J. Maris, F. Ancilotto, M. Barranco, M. Pi, and D. Mateo for helpful discussions. This work was supported in part by the National Science Foundation through Grant No. DMR-0605355.

[1] W. T. Sommer, Phys. Rev. Lett. **12**, 271 (1964); M. A. Woolf and G. W. Rayfield, *ibid.* **15**, 235 (1965); J. Classen, C.-K. Su, M. Mohazzab, and H. J. Maris, Phys. Rev. B **57**, 3000 (1998).

[2] B. E. Springett, M. H. Cohen, and J. Jortner, Phys. Rev. **159**, 183 (1967); Y. M. Shih and C.-W. Woo, Phys. Rev. A **8**, 1437 (1973).

[3] L. Meyer and F. Reif, Phys. Rev. **110**, 279 (1958); F. Reif and L. Meyer, *ibid.* **119**, 1164 (1960).

[4] A. Phillips and P. V. E. McClintock, Phys. Rev. Lett. **33**, 1468 (1974).

[5] R. M. Bowley, P. V. E. McClintock, F. E. Moss, and P. C. E. Stamp, Phys. Rev. Lett. **44**, 161 (1980); G. G. Nancolas and P. V. E. McClintock, *ibid.* **48**, 1190 (1982).

[6] G. W. Rayfield and F. Reif, Phys. Rev. **136**, A1194 (1964).

[7] D. M. Strayer and R. J. Donnelly, Phys. Rev. Lett. **26**, 1420 (1971).

[8] G. G. Nancolas, T. Ellis, P. V. E. Mclintock, and R. M. Bowley, Nature (London) **316**, 797 (1985).

[9] K. W. Schwarz and P. S. Jang, Phys. Rev. A **8**, 3199 (1973); C. M. Muirhead, W. F. Vinen, and R. J. Donnelly, Philos. Trans. R. Soc. London, Ser. A **311**, 433 (1984).

[10] R. J. Donnelly, *Quantizd Vortices in Helium II* (Cambridge University Press, Cambridge, 1991).

[11] A. F. Borghesani, *Electrons and Ions in Liquid Helium* (Oxford University Press, New York, 2007).

[12] T. Frisch, Y. Pomeau, and S. Rica, Phys. Rev. Lett. **69**, 1644 (1992); T. Winiecki, J. F. McCann, and C. S. Adams, Europhys. Lett. **48**, 475 (1999); T. Winiecki and C. S. Adams, *ibid.* **52**, 257 (2000).

[13] N. G. Berloff and P. H. Roberts, Phys. Rev. B **63**, 024510 (2000); J. Phys. A **34**, 81 (2001); N. G. Berloff and C. F. Barenghi, Phys. Rev. Lett. **93**, 090401 (2004).

[14] N. G. Berloff and P. H. Roberts, J. Phys. A **32**, 5611 (1999).

[15] F. Dalfovo, A. Lastri, L. Pricaupenko, S. Stringari, and J. Treiner, Phys. Rev. B **52**, 1193 (1995).

[16] L. Giacomazzi, F. Toigo, and F. Ancilotto, Phys. Rev. B **67**, 104501 (2003); F. Ancilotto, F. Dalfovo, L. P. Pitaevskii, and F. Toigo, *ibid.* **71**, 104530 (2005); D. Mateo, M. Pi, and M. Barranco, *ibid.* **81**, 174510 (2010).

[17] S. Stringari and J. Treiner, Phys. Rev. B **36**, 8369 (1987).

[18] D. Jin and H. J. Maris, J. Low Temp. Phys. **158**, 317 (2010).

[19] K. Penanen, M. Fukuto, R. K. Heilmann, I. F. Silvera, and P. S. Pershan, Phys. Rev. B **62**, 9621 (2000).

[20] H. J. Maris, J. Low Temp. Phys. **94**, 125 (1994); F. Dalfovo, Phys. Rev. B **46**, 5482 (1992).

[21] W. Guo and H. J. Maris, *Proceedings of the 24th International Conference on Low Temperature Physics*, AIP Conf. Proc. No. 850 (AIP, New York, 2006), p. 161.

[22] See supplementary material at http://link.aps.org/supplemental/10.1103/PhysRevB.82.094524 for the continuous movie.